Automatic calibration of damping layers in finite element time domain simulations

Steven Vandekerckhove* Garth N. Wells† Herbert De Gersem‡
Koen Van Den Abeele§

arXiv:1601.07941v1 [cs.CE] 28 Jan 2016

Abstract

Matched layers are commonly used in numerical simulations of wave propagation to model (semi-)infinite domains. Attenuation functions describe the damping in layers, and provide a matching of the wave impedance at the interface between the domain of interest and the absorbing region. Selecting parameters in the attenuation functions is non-trivial. In this work, an optimisation procedure for automatically calibrating matched layers is presented. The procedure is based on solving optimisation problems constrained by partial differential equations with polynomial and piecewise-constant attenuation functions. We show experimentally that, for finite element time domain simulations, piecewise-constant attenuation function are at least as efficient as quadratic attenuation functions. This observation leads us to introduce consecutive matched layers as an alternative to perfectly matched layers, which can easily be employed for problems with arbitrary geometries. Moreover, the use of consecutive matched layers leads to a reduction in computational cost compared to perfectly matched layers. Examples are presented for acoustic, elastodynamic and electromagnetic problems. Numerical simulations are performed with the libraries FEniCS/DOLFIN and dolfin-adjoint, and the computer code to reproduce all numerical examples is made freely available.

1 Introduction

Three types of boundary conditions are frequently used in numerical wave propagation problems: reflecting boundaries, modelled by homogeneous Dirichlet and Neumann conditions; ports through which energy enters or leaves the system, modelled by non-homogeneous Dirichlet or Neumann boundary conditions; and boundary conditions that mimic open space when truncating an infinite domain. A number of strategies for truncating infinite domains have been developed, including absorbing boundary conditions [15, 26], absorbing layers [17, 20] and one-way approximations [10, 23]. An absorbing layer introduces damping and is realised by extending the computational domain beyond the domain of interest, and it is desirable to keep the size of the absorbing domain as small as possible to limit the additional computational work. However, none of the early damping layer techniques proved to be flawless.

In 1994, Bérenger [4] introduced an absorbing domain called Perfectly Matched Layers (PMLs). In a PML, waves are damped at a certain rate, described by an attenuation function (AF). It is desirable to use an 'optimal' AF in order to limit the size of the PML. Unfortunately, there is no universal recipe available to determine the best AF for specific problems. For particular cases, optimal PMLs can be found through mathematical analysis. For example, Chew and Jin [7] proved that for finite difference time domain methods, second-order polynomial AFs are optimal and suggested that these results should also be expected for finite element time domain methods. A generalisation of the analysis to more complicated cases (unstructured meshes, more general geometries and loads) is not straightforward, may be suboptimal or may even fail.

In this work we present an automatic calibration procedure for PMLs through optimisation of the PML parameters for a given problem. The functional we attempt to minimise is the energy left in the domain after an input signal should have left the domain of interest. The problem is constrained by the considered differential equation that describes the wave propagation of interest. We use gradient-based optimisation procedures to determine the parameters, with the adjoint of the forward problem used to compute the derivative of the target functional with respect to the PML parameters. We consider polynomial and piecewise-constant AFs, with the latter case motivating the introduction of what we will call 'Consecutive Matched Layers' (CMLs). An advantage of CMLs is that they are easily added to problems with arbitrary geometries, as we will show through numerical examples.

*Wave Propagation and Signal Processing Research Group, KU Leuven - Kulak, Etienne Sabbelaan 53, 8500 Kortrijk, Belgium
†Department of Engineering, University of Cambridge, Trumpington Street, Cambridge CB2 1PZ, United Kingdom
‡Institut für Elektromagnetischer Felder, Technische Universität Darmstadt, Schlossgartenstrasse 8, 64289 Darmstadt. Germany
§Wave Propagation and Signal Processing Research Group, KU Leuven - Kulak, Etienne Sabbelaan 53, 8500 Kortrijk, Belgium

Numerical examples of the proposed procedure are presented for acoustic, elastodynamic and electromagnetic problems. The examples use the FEniCS/DOLFIN [21, 22, 2] and dolfin-adjoint [12, 13] libraries. The complete source code to produce the presented examples is freely available and provided as supporting material [30].

The remainder of the paper is organised as follows. The considered wave propagation problems are described in Section 2, followed by the introductions of PMLs in Section 3. In Section 4, the formulation of Consecutive Matched Layers (CMLs) is presented, which is followed by the proposed procedure for automatic calibration of PMLs and CMLs in Section 5. We present and discuss test cases and results in Section 6. Conclusions are drawn in Section 7.

2 Wave propagation problems

We will consider acoustic, elastodynamic and electromagnetic wave propagation problems. Each of these problems is defined in this section, but we first present a generic formulation in which these problems can framed.

On a spatial domain $\Omega \subset \mathbb{R}^d$, where $1 \leq d \leq 3$, we consider linear wave propagation problems in the generic form

$$\dot{\boldsymbol{q}} + \sum_{i=1}^{d} \boldsymbol{F}_{i,i} = \boldsymbol{f} \qquad \text{on } \Omega \times [0,\, T], \tag{1}$$

where $\boldsymbol{q}$ is a vector of length n containing the n unknown fields, $\boldsymbol{F}_i = \boldsymbol{A}_i \boldsymbol{q}$ is a flux vector of length n, $\boldsymbol{f}$ is a source function of length n and T is the final time. The matrices $\boldsymbol{A}_i$ contain material parameters and will be defined for each specific problem we consider. The notation $\boldsymbol{F}_{i,i} = \partial \boldsymbol{F}_i / \partial x_i$ (no summation) implies component-wise partial differentiation of $\boldsymbol{F}_i$ with respect to x_i. Boundary conditions will be presented later for each specific problem.

The first considered model is acoustic wave propagation, described by the system

$$\begin{aligned} \frac{1}{K}\dot{p} &= -\nabla \cdot \boldsymbol{v}, \\ \rho \dot{\boldsymbol{v}} &= -\nabla p + \boldsymbol{f}, \end{aligned} \tag{2}$$

where $K > 0$ is the bulk modulus, p is the pressure, $\boldsymbol{v}$ is the velocity, $\rho > 0$ is the mass density and $\boldsymbol{f}$ is an applied body force. This problem is transformed into the generic form (1), in three-dimensions, with $\boldsymbol{q} = (v_1, v_2, v_3, p)^T$ and the matrices $\boldsymbol{A}_i$ in (31).

The second model concerns electromagnetic wave propagation, described by the system

$$\begin{aligned} \mu \dot{\boldsymbol{H}} &= -\nabla \times \boldsymbol{E}, \\ \varepsilon \dot{\boldsymbol{E}} &= \nabla \times \boldsymbol{H} - \boldsymbol{J}, \end{aligned} \tag{3}$$

where $\mu > 0$ is the permeability, $\boldsymbol{H}$ is the magnetic field strength, $\boldsymbol{E}$ is the electric field strength, $\varepsilon > 0$ is the permittivity and $\boldsymbol{J}$ is a current density. This problem is transformed into the generic form (1), in three dimensions, with $\boldsymbol{q} = (H_1, H_2, H_3, E_1, E_2, E_3)^T$ and the matrices $\boldsymbol{A}_i$ in (34).

Finally, linearised elastic wave propagation will be considered, and is described by the system

$$\begin{aligned} \boldsymbol{\mathcal{C}}^{-1} : \dot{\boldsymbol{T}} &= \frac{1}{2}\left(\nabla \boldsymbol{v} + (\nabla \boldsymbol{v})^T\right), \\ \rho \dot{\boldsymbol{v}} &= \nabla \cdot \boldsymbol{T} + \boldsymbol{f}, \end{aligned} \tag{4}$$

where $\boldsymbol{\mathcal{C}}$ is the fourth-order, isotropic elastic stiffness tensor, $\boldsymbol{T}$ is the stress tensor, $\boldsymbol{v}$ is the particle velocity, $\rho > 0$ the mass density and $\boldsymbol{f}$ is an applied body force. This problem is transformed into the generic form (1), in three dimensions, with $\boldsymbol{q} = (v_1, v_2, v_3, T_{11}, T_{22}, T_{33}, 2T_{23}, 2T_{13}, 2T_{12})^T$ and the matrices $\boldsymbol{A}_i$ in (37).

3 Perfectly matched layers

We denote the domain of physical interest by Ω_i, which is extended with an absorbing domain Ω_a ($\Omega_i \cap \Omega_a = \emptyset$), leading to the computational domain $\Omega = \Omega_i \cup \Omega_a$. To obtain a formulation for wave propagation problems with PMLs, we apply the technique of complex coordinate stretching [8, 28] to the generic wave equation in (1).

Solutions to wave equations are of the form

$$\boldsymbol{q}(\boldsymbol{x}, t) = \bar{\boldsymbol{q}}\,(\boldsymbol{x})\, e^{-\jmath \omega t}, \tag{5}$$

where $\bar{\boldsymbol{q}}(\boldsymbol{x})$ is the spatial solution and ω is the frequency. A frequency domain formulation can be used by noting that $\dot{\boldsymbol{q}} = -\jmath\omega \boldsymbol{q}$. PMLs in all directions are applied by introducing the coordinate transformations

$$\frac{\partial}{\partial x_i} \rightarrow \left(\frac{1}{1 + \jmath \frac{\sigma_i(x_i)}{\omega}}\right) \frac{\partial}{\partial x_i}, \tag{6}$$

where $\sigma_i(x_i)$ are attenuation functions (AFs), and which are non-zero only in the absorbing region Ω_a. The AFs will be defined at the end of the section.

We will denote combinations of different AFs in the index, e.g. $\sigma_{ij+k} = \sigma_i\sigma_j + \sigma_k$. Using (5) and applying the coordinate transformations in (6) to the wave equation (1) leads to

$$-\jmath\omega\boldsymbol{q} + \sum_{i=1}^{d} \frac{\boldsymbol{F}_{i,i}}{1 - \frac{\sigma_i}{\jmath\omega}} = \boldsymbol{f}. \tag{7}$$

Multiplying (7) by all denominators appearing in it leads to

$$-\jmath\omega\left(\prod_{i=1}^{d}\left(1-\frac{\sigma_i}{\jmath\omega}\right)\right)\boldsymbol{q} + \sum_{i=1}^{d}\left(\prod_{\substack{j=1\\j\neq i}}^{d}\left(1-\frac{\sigma_j}{\jmath\omega}\right)\right)\boldsymbol{F}_{i,i} = \left(\prod_{i=1}^{d}\left(1-\frac{\sigma_i}{\jmath\omega}\right)\right)\boldsymbol{f}. \tag{8}$$

With no source term inside the absorbing region Ω_a, we have $\sigma_i\boldsymbol{f} = \boldsymbol{0}$ and the right-hand side of (8) simplifies to $\boldsymbol{f}$. Expanding the remaining products leads to

$$\begin{aligned}-\jmath\omega\boldsymbol{q} + \sum_{i=0}^{3}\boldsymbol{F}_{i,i} + \sigma_{1+2+3}\boldsymbol{q} - \frac{1}{\jmath\omega}\sigma_{12+13+23}\boldsymbol{q} + \frac{1}{(\jmath\omega)^2}\sigma_{123}\boldsymbol{q} - \frac{1}{\jmath\omega}\sum_{i=0}^{3}\left(\sum_{\substack{j=1\\j\neq i}}^{d}\sigma_j\right)\boldsymbol{F}_{i,i}\\ + \frac{1}{(\jmath\omega)^2}\sum_{i=0}^{3}\left(\prod_{\substack{j=1\\j\neq i}}^{d}\sigma_j\right)\boldsymbol{F}_{i,i} = \boldsymbol{f}.\end{aligned} \tag{9}$$

To obtain a system of first-order equations from (9), for $d = 3$ two auxiliary fields, $\dot{\boldsymbol{r}} = \boldsymbol{q}$ and $\dot{\boldsymbol{s}} = \boldsymbol{r}$ are introduced, resulting in two auxiliary differential equations (ADEs) in addition to the wave equation:

$$\begin{aligned}\dot{\boldsymbol{q}} + \boldsymbol{F}_{1,1} + \boldsymbol{F}_{2,2} + \boldsymbol{F}_{3,3} + \sigma_{1+2+3}\boldsymbol{q} + \boldsymbol{r} &= \boldsymbol{f},\\ \dot{\boldsymbol{r}} - \sigma_{12+13+23}\boldsymbol{q} - \sigma_{2+3}\boldsymbol{F}_{1,1} - \sigma_{1+3}\boldsymbol{F}_{2,2} - \sigma_{1+2}\boldsymbol{F}_{3,3} - \boldsymbol{s} &= \boldsymbol{0},\\ \dot{\boldsymbol{s}} + \sigma_{123}\boldsymbol{q} + \sigma_{23}\boldsymbol{F}_{1,1} + \sigma_{13}\boldsymbol{F}_{2,2} + \sigma_{12}\boldsymbol{F}_{3,3} &= \boldsymbol{0}.\end{aligned} \tag{10}$$

In two spatial dimensions ($d = 2$) , we have the simplified system:

$$\begin{aligned}\dot{\boldsymbol{q}} + \boldsymbol{F}_{1,1} + \boldsymbol{F}_{2,2} + \sigma_{1+2}\boldsymbol{q} + \boldsymbol{r} &= \boldsymbol{f},\\ \dot{\boldsymbol{r}} - \sigma_2\boldsymbol{F}_{1,1} + \sigma_1\boldsymbol{F}_{2,2} - \sigma_{12}\boldsymbol{q} &= \boldsymbol{0}.\end{aligned} \tag{11}$$

In one spatial dimension ($d = 1$), there are no ADEs needed to describe the PML:

$$\dot{\boldsymbol{q}} + \boldsymbol{F}_{1,1} + \sigma_1\boldsymbol{q} = \boldsymbol{f}. \tag{12}$$

A specific PML is defined by the AFs σ_i. The literature, e.g. [7], generally suggests polynomial AFs. For axis-aligned rectangular (cuboid) domains, polynomial AFs can be expressed as

$$\sigma_i(x_i) = \begin{cases}\sum_{j=0}^{n} c_{ij}\bar{x}_i^j & \text{if } x_i \in [a_{(i)0}, a_{(i)0} + w_i]\\ 0 & \text{otherwise,}\end{cases} \tag{13}$$

where n is the order of the polynomial, c_{ij} are the coefficients of the polynomial, $\bar{x}_i = g(x_i)$ is an affine transformation of x_i such that $g(x_i) = 0$ on the boundary between the domain of interest and the absorbing region, and $g(x_i) = 1$ on the exterior boundary of the absorbing region, $x_i = a_{(i)0}$ is the interface between Ω_i and Ω_a and w_i is the total width of the PML in the ith direction.

We also introduce a description of an AF with N piecewise-constant AFs of the form

$$\sigma_i(x_i) = \begin{cases}c_{ij} & \text{if } x_i \in [a_{(i)j}, a_{(i)j+1}]\ \forall j = 0 \ldots N-1,\\ 0 & \text{otherwise,}\end{cases} \tag{14}$$

where $c_{ij} \geq 0$ are scalar values and $a_{(i)j} = a_i + j(w_i/N)$.

4 Consecutive matched layers

The complex coordinate stretching procedure used in the previous section to the PML configuration depicted in Figure 1a. Overlapping PML regions leads to products of AFs that appear in the ADEs in (10). Solving for the auxiliary fields adds to the computational cost. To avoid this increase in cost, we adopt a simplification to the PML strategy.

When using non-overlapping absorbing domains, as depicted in Figure 1b, products of AFs are zero and (10) reduces to

$$\begin{aligned} \dot{\boldsymbol{q}} + \boldsymbol{F}_{1,1} + \boldsymbol{F}_{2,2} + \boldsymbol{F}_{3,3} + \sigma_{1+2+3}\boldsymbol{q} + \boldsymbol{r} &= \boldsymbol{f}, \\ \dot{\boldsymbol{r}} - \sigma_{2+3}\boldsymbol{F}_{1,1} - \sigma_{1+3}\boldsymbol{F}_{2,2} - \sigma_{1+2}\boldsymbol{F}_{3,3} &= \boldsymbol{0}, \end{aligned} \tag{15}$$

which eliminates one ADE compared to (10). If we assume that $\boldsymbol{r} = \boldsymbol{0}$, which can be motivated by the fact that spatial derivatives in the second equation will be relatively small due to the damping, also the second ADE vanishes, further reducing (10) to

$$\dot{\boldsymbol{q}} + \boldsymbol{F}_{1,1} + \boldsymbol{F}_{2,2} + \boldsymbol{F}_{3,3} + \sigma_{1+2+3}\boldsymbol{q} = \boldsymbol{f}. \tag{16}$$

Since we prefer direction-independent AFs, we choose the AF in all directions to be defined by the same constant. Hence, σ_{1+2+3} can be replaced by an AF of the form

$$\sigma_i(\boldsymbol{x}), = \begin{cases} c_i & \text{if } \boldsymbol{x} \in \Omega_{a_i} \\ 0 & \text{otherwise,} \end{cases} \tag{17}$$

where $c_i \geq 0$ is a constant scalar and Ω_{a_i} is the ith 'layer' of the absorbing domain. Using the AF in (17) for a problem where $\Omega_{a_1} = \Omega_a$ leads to a simplification of (16):

$$\dot{\boldsymbol{q}} + \boldsymbol{F}_{1,1} + \boldsymbol{F}_{2,2} + \boldsymbol{F}_{3,3} + \sigma\boldsymbol{q} = \boldsymbol{f}. \tag{18}$$

This formulation closely resembles the original absorbing layer strategy [17]. We however suggest to consider an absorbing domain Ω_a which is divided into N non-overlapping absorbing layers Ω_{a_i} such that $\Omega_a = \bigcup_{i=1}^{N} \Omega_{a_i}$, which leads to the formulation

$$\dot{\boldsymbol{q}} + \boldsymbol{F}_{1,1} + \boldsymbol{F}_{2,2} + \boldsymbol{F}_{3,3} + \sigma_i(\boldsymbol{x})\boldsymbol{q} = \boldsymbol{f}, \tag{19}$$

The resulting configuration is illustrated in Figure 1c, where the AF is constant on each colour/layer. Due to the absence of auxiliary fields, the computational cost is reduced relative to the PML model. A difficulty is how to choose the terms that define the AFs in the layers. This issue will be addressed in the following section.

We note that a reasonable domain of interest can be extended with tightly wrapped layers, as shown in Figure 1d, and meshed conformingly. Hence this procedure can be applied to problems with arbitrary geometries, while avoiding complex mathematical interventions, e.g., as presented in [14].

By neglecting the ADE in (15) the absorbing domain is no longer a PML, hence we will refer to the simplified damping strategy as *consecutive matched layers* (CMLs). This name refers to the non-reflective free space boundary condition introduced in Katz et al. [20], mentioned as *absorbing layer* in Holland and Williams [17] and referred to as *matched layer* in Bérenger [4].

5 Automatic calibration of matched layer problems

The matched layer approaches presented in the preceding sections involved scalar AFs, $\sigma_i\,(x_i)$, and it is necessary to define their functional form. For finite difference methods, there are numerous papers describing how to determine the AFs, e.g, [3, 7, 9]. Chew and Jin [7] proved that quadratic polynomials result in optimal AFs for finite difference methods. Even if we presume that quadratic polynomial AFs are optimal for finite element time domain simulations, the question remains what precise form the quadratic polynomial should take for optimal results. Since users often want to add damping layers to their models without studying the truncation strategy in depth, an automatic determination procedure is appealing. We present a generic recipe for automatic calibration of the AF coefficients. The presented procedure is based on solving an optimisation problem.

5.1 Formulation of the optimisation problem

Our abstract optimisation problem is formulated as

$$\min_{\boldsymbol{y},\boldsymbol{u}} J(\boldsymbol{y},\boldsymbol{u}) \qquad \text{(objective functional)}, \tag{20}$$

$$\boldsymbol{c}(\boldsymbol{y},\boldsymbol{u}) = \boldsymbol{0} \qquad \text{(constraint)}, \tag{21}$$

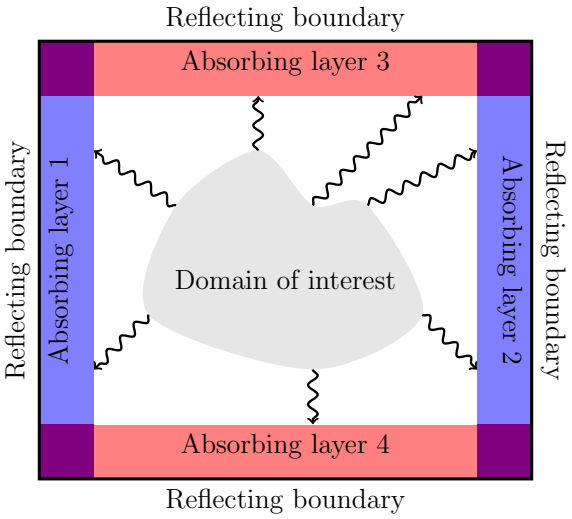

(a) Adding perfectly matched layers in multiple directions to a geometry using complex coordinate stretching leads to overlapping regions.

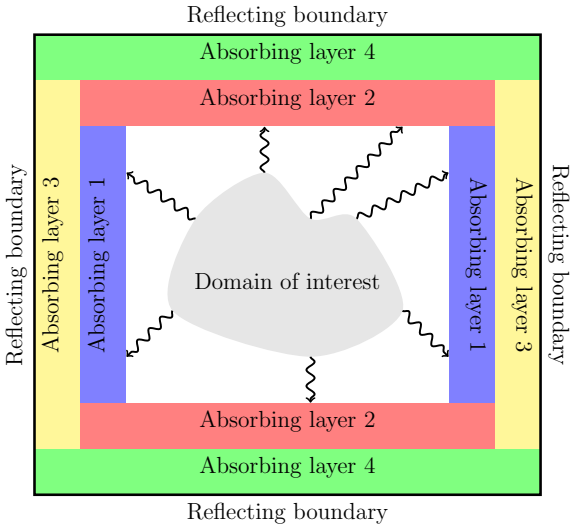

(b) Multiple perfectly matched layers that have been added to a geometry without overlap.

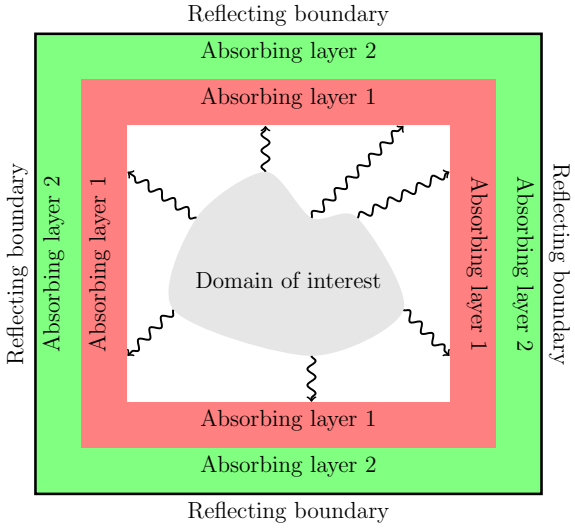

(c) When two consecutive layers as shown in Figure 1b are defined by the same constant value, they can be considered as one merged layer. Fragmentation of a matched layer in this manner can be used to add tightly wrapped absorbing layers to an arbitrary geometry, as demonstrated in Figure 1d.

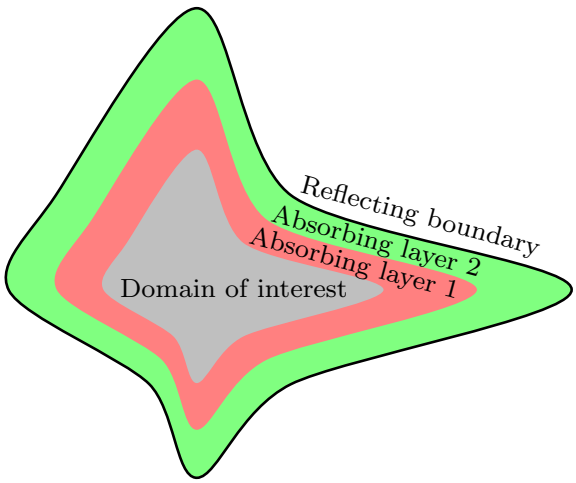

(d) Multiple tightly wrapped absorbing layers around an arbitrary geometry.

Figure 1: Graphical depiction of perfectly matched layers and consecutive matched layers.

where J is a scalar function, $\boldsymbol{y}$ is the state vector, $\boldsymbol{u} \in U_{\text{ad}}$ is the control vector, U_{ad} is the set of the admissible values for the control values and $\boldsymbol{c}$ represents a set of constraints. For the considered problems, the state vector $\boldsymbol{y}$ contains $\boldsymbol{q}$ in the wave equation (1), and in the case of PML calibration is also contains the solutions of the auxiliary fields $\boldsymbol{r}$ and $\boldsymbol{s}$ in (10). The control vector $\boldsymbol{u}$ contains the c_{ij} parameters that define the AFs. Satisfaction of the constraint $\boldsymbol{c}(\boldsymbol{y}, \boldsymbol{u})$ in our case is satisfaction of the wave equation with matched layers.

The matched layer optimisation problem is in general not convex due to the non-linear relation between the controls and the states given by the constraint. This implies the likely existence of multiple local minima. Consequences of the existence of multiple local minima will be demonstrated by the numerical examples in Section 6. This prohibits us of considering the outcome of the automatic calibration procedure as optimal. Based on experimental results, we will however argue that the outcome is very likely to have near optimal performance.

5.2 Measuring the quality of the absorbing region

To define an objective functional we need to quantify the quality of a matched layer problem. Typical quality measures involve the reflection coefficients, both at the interface between the domain of interest Ω_i and the matched layer Ω_a, and within the matched layer (see [7]). This *a priori* quality measure is difficult to manipulate in combination with finite element formulations.

We propose quantifying the quality of a matched layer through the amount of energy in a system at judiciously chosen time for a judiciously chosen source term. With reflecting boundaries around the domain of interest and a vanishing input signal, the total energy in the system for the considered problems is constant once the input signal has vanished. If the domain of interest was embedded in an infinite domain, the total energy in the domain of interest would be zero at sufficiently large time. When absorbing layers are added to the domain of interest to mimic an infinite domain, the energy will reduce over time due to attenuation in the absorbing layers only, but it is highly unlikely that it will ever be exactly zero. The goal of the calibration procedure is to choose parameters for the matched layers such that the energy in the whole computational domain is minimised at a suitably chosen time, which we will call the 'calibration time', T_c. The reduction in energy in the numerical simulation at time T due to the absorbing layers is given by

$$\delta E = -10 \log_{10} \left(\frac{E\left(T\right)}{\bar{E}\left(T\right)} \right), \tag{22}$$

where $\bar{E}$, the energy in the whole computational domain with zero-valued AFs, is used as a reference value and E is the energy on the computational domain for the problem with non-zero AFs.

For the problems that we consider, the energy in a system is given by:

$$E(t) = \frac{1}{2} \left\langle \boldsymbol{Q}\boldsymbol{q}(t), \boldsymbol{q}(t) \right\rangle_{\Omega}, \tag{23}$$

where $\langle ., . \rangle_{\Omega}$ is the L_2 inner product over the entire computational domain Ω and $\boldsymbol{Q}$ is a matrix containing the material parameters. Concrete expressions for the energy and the matrices $\boldsymbol{Q}$ for the specific problems in Section 2 are given in A.

5.3 Objective functional

The objective functional we use in calibrating matched layer problems is

$$J(\boldsymbol{q}, \boldsymbol{u}) = E(T_c), \tag{24}$$

where $E(T_c)$ is the energy in the system at the calibration time.

Another quantity of interest in designing matched layers is reflections at the interface between the domain of interest and the damping region. If the calibration time T_c is chosen too large, then energy can be damped gradually every time a wave encounters the damping region and is partially reflected by it. In order to include the effect of these reflections in J (24), the calibration time should be chosen such that reflections of the input signal at the material/matched layer interface encounter the damping region as few times as possible.

A practical concern is that the calibration time should be chosen as small as possible for computational speed, since a greater calibration time increases the number of time steps, and hence the cost of the optimisation process.

5.4 Computing derivatives of the objective functional

We will use derivative-based optimisation methods to calibrate the matched layer parameters. To compute the gradient of the objective functional J with respect to the control parameters $\boldsymbol{u}$, we use the adjoint approach [29].

In essence, we find $\mathrm{d}J/\mathrm{d}\boldsymbol{u}$ from

$$\frac{\mathrm{d}J}{\mathrm{d}\boldsymbol{u}} = \frac{\partial J}{\partial \boldsymbol{u}} - \boldsymbol{\lambda}^T \frac{\mathrm{d}\boldsymbol{c}}{\mathrm{d}\boldsymbol{u}}, \tag{25}$$

where the adjoint variable $\boldsymbol{\lambda}$ is the solution to:

$$\left(\frac{\partial \boldsymbol{c}}{\partial \boldsymbol{q}}\right)^T \boldsymbol{\lambda} = \left(\frac{\partial J}{\partial \boldsymbol{q}}\right)^T. \tag{26}$$

A detailed derivation for the time discretised problems can be found in C. Key to the adjoint approach for computing derivatives of functionals is that that only one system needs to be solved to compute the gradient, regardless of the number of controls. Moreover, (26) is similar in structure to the system that is solved in the forward problem.

For the numerical examples in Section 6, in our implementations we express the forward model in FEniCS syntax [1, 21, 22], from which the adjoint problem is computed automatically by the library dolfin-adjoint [13].

5.5 Practical procedure

To automatically calibrate a PML or CMLs for a problem of interest we create a calibration set-up. The procedure is:

1. Extend the domain of interest with artificial layers Ω_a and mesh domain with cell edges conforming to the boundary of Ω_i and Ω_a.
2. Extend the physical material parameters on the domain of interest to the absorbing region.
3. Set the attenuation in the damping region to zero.
4. Select an input signal with local support in time to fit the frequency range of the application under consideration.
5. Select a calibration time T_c, such that the peak of the input pulse has travelled at least once through the damping region in every direction at the lowest wave speed.
6. Update the AF parameters via a gradient-based optimisation process.

When the optimiser has converged, the obtained controls for the calibration set-up are used in the AF to solve the forward problem of interest. Note that the calibration set-up can differ from the problem of interest, as will be demonstrated for the electromagnetic example in Section 6. In the other example the geometry, mesh and excitation of the problem of interest and calibration set-up are kept. The final time of the problem of interest can differ from the calibration time, T_c. We will call the final time for the problem of interest the 'evaluation time', T_e.

6 Numerical examples and discussion

We present examples using the calibration procedure for finite element acoustic, elastic and electromagnetic wave propagation problems, and consider both PMLs and CMLs. We will begin with a one-dimensional example, before moving on to two- and three-dimensional cases to examine performance with oblique incidence angles. We will consider PMLs for acoustic and elastodynamic examples, and CMLs for elastodynamic and electromagnetic examples. The computer code for reproducing all examples is available in the supporting material [30].

For all examples, we use the L-BFGS-B optimiser from SciPy [19]. This optimiser is a limited memory BFGS implementation with bound support [6]. The bound support is used to prevent the optimiser choosing negative values for the piecewise-constant AFs. The optimiser stops when the gradient drops below a chosen threshold [25]. The threshold used in the different examples can be found in the supporting material [30].

To fully define the objective functional in (24), a calibration time and input signal have to be chosen. For all examples we use a Gaussian pulse. We choose the calibration time such that the peak of the input pulse has time to travel at least once to the boundary of the computational domain and back to the interface between the domain of interest and the absorbing domain at the lowest wave speed. Unless mentioned otherwise, first-order elements are used for all computations.

6.1 Perfectly matched layers

The examples presented in this section consider polynomial and piecewise-constant AFs for PMLs, as described in Section 3.

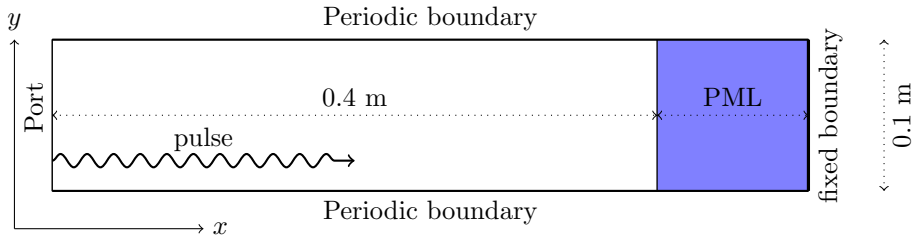

Figure 2: Geometry of the two-dimensional acoustic wave example with waves propagating in one direction.

6.1.1 Acoustic wave propagation

We consider a rectangular domain of interest $\Omega_i = [0, 0.4]$ m $\times$ $[0, 0.1]$ m, which is extended at the right-hand boundary with a PML, as depicted in Figure 2. The domain is meshed with crossed-triangle cells with edge length 0.01 m in both x- and y-directions. Periodic boundary conditions are applied in the y-direction. On the right-hand side of the computational domain, a reflecting boundary condition with $\boldsymbol{v} = \boldsymbol{0}$ is applied. An open boundary on the right-hand side of the domain is modelled by adding a PML in front of the reflecting boundary. On the left-hand boundary, the condition $\boldsymbol{v} = \left(\exp\left(-\left(4(t-t_0)/t_0\right)^2\right), 0\right)$ m/s is applied, where t_0 is the offset for the pulse. Note that for a large enough time $\boldsymbol{v}$ approaches zero and this boundary acts as a reflecting fixed boundary. We consider a homogeneous medium with mass density $\rho = 1.269$ kg/m^3 and bulk modulus $K = 101000$ Pa. The time step is 90% of the CFL condition, $\Delta t = 0.9 \times 0.01/(v\sqrt{2})$ s, where $v = \sqrt{K/\rho}$ is the wave speed for the medium. The offset of the pulse is chosen to be $t_0 = 100\Delta t$. The calibration time T_c is chosen to be the time the peak of the pulse needs to travel two and a half times through the domain of interest, $T_c = 2.5(0.4\text{m})v + t_0$. This way the peak of the pulse can encounter the PML interface only once, but there is sufficient time for the pulse to travel back-and-forth in the PML. For this example the calibration set-up is identical to the problem of interest, including the evaluation time $T_e = T_c$.

We first compare constant with piecewise-constant AFs for different PML widths. The smallest considered PML is 0.01 m wide. The PML is extended 0.01 m in x-direction seventeen times, up to a total width of 0.18 m. When a piecewise-constant AF is considered, one control value is added for every extension, e.g., for a 0.05 m wide PML, the piecewise-constant AF is defined by five control variables. The energy reduction, as defined in (22), for these experiments with the calibrated AFs is shown in Figure 3a. These results show that piecewise-constant AFs perform better than constant AFs for every PML width.

The reduction in energy for different polynomial order AFs and different PML widths is shown in Figure 3b. First note the results for the fourth-order polynomial AF, where the 0.10 m PML appears to outperform the 0.15 m PML. This peculiarity points to the optimisation problem being non-convex. We will comment on this further when examining initial guesses for the controls. Comparing Figure 3a and Figure 3b, it can be concluded that piecewise-constant AFs outperform the polynomial AFs, e.g., for a 0.10 m wide PML, the calibrated piecewise-constant AF reduces the energy more than any polynomial AF. We note from Figure 3b that there appears to be limited benefit in using polynomial orders greater than two, which is consistent with finite difference results presented by Chew and Jin [7]. We restrict further experiments to AFs to polynomial degrees of two or less.

We would expect the performance of a polynomial AF to be at least as good as the constant AF case since the polynomial case contains the constant case. However, Figure 3b shows that for a 0.05 m wide PML, a constant AF is slightly more effective than any other polynomial AF. This again points to the optimisation problem being non-convex.

We now fix the PML width to 0.05 m to examine the influence of the initial AF parameters. Figure 4 shows the reduction in energy after optimisation for zero initial values (index 0) and random starting values (indices greater than zero) for both a piecewise-constant and a quadratic AF. The starting values are uniformly sampled on the interval $[0, 7000]$ for the piecewise-constant case and the interval $[-500, 500]$ for the polynomial case. For the polynomial case, we allow negative coefficients in order to allow AFs that are not monotonically increasing. For the piecewise-constant AFs, the energy reduction for approximately ten percent of the results is more than 10 dB from the best result. There is less variation in the computed energy reduction for quadratic AFs compared to the piecewise-constant case. However, every piecewise-constant AF outperforms all quadratic AFs. In the remainder we will set the initial guess for all controls to zero.

Figure 5 shows the piecewise-constant AF for 0.02 m, 0.05 m, 0.10 m, 0.15 m and 0.19 m wide PMLs. The result is not immediately intuitive; the first control value is relatively large, followed by a substantially smaller second control value. The remaining control values are approximately equal and larger than the second value. The counter-intuitive outcome highlights an advantage of using an optimisation approach.

Figure 6 shows how the control values of the piecewise-constant AF change with each optimiser iteration for

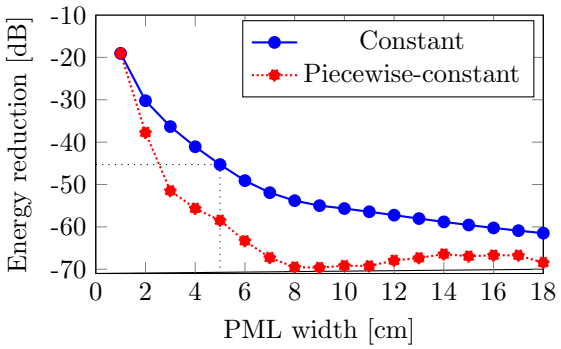

(a) The solid blue curve shows the energy reduction for a constant attenuation function, and the dotted red curve for a piecewise-constant attenuation function as explained in Section 3.

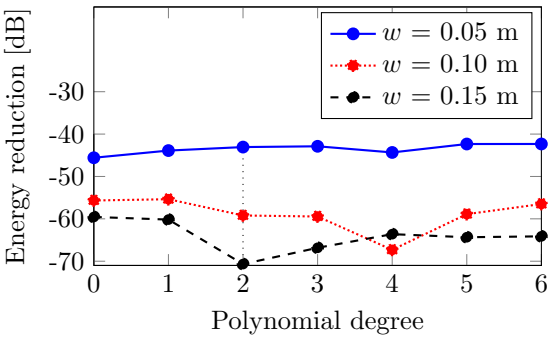

(b) Perfectly matched layers are considered with three different widths w.

Figure 3: Energy reduction with perfectly matched layers for the acoustic wave example depending on the perfectly matched layer width (left) and polynomial degree for the attenuation function (right).

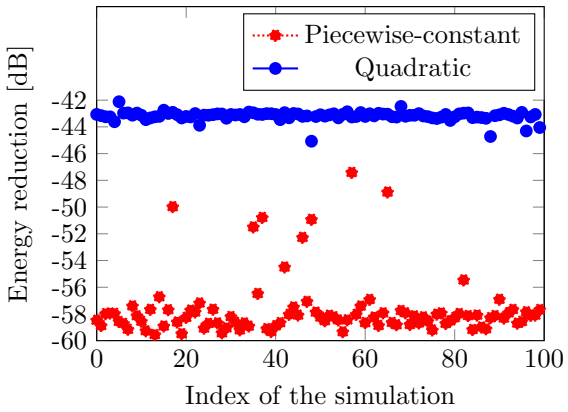

Figure 4: Energy reduction achieved by the calibrated attenuation functions for the acoustic wave example with zero initial values (index 0) and random sets of initial values (index > 0). The perfectly matched layer is 0.05 m wide. The experiment was performed for quadratic (dotted red) and piecewise-constant attenuation functions (solid blue).

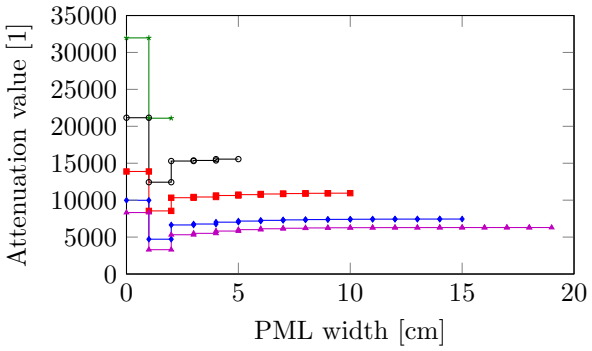

Figure 5: Optimal piecewise-constant attenuation functions for perfectly matched layers for the acoustic wave example for the case of 0.02 m (green stars), 0.05 m (black circles), 0.10 m (red squares), 0.15 m (blue diamonds) and 0.19 m (purple triangles) wide perfectly matched layer.

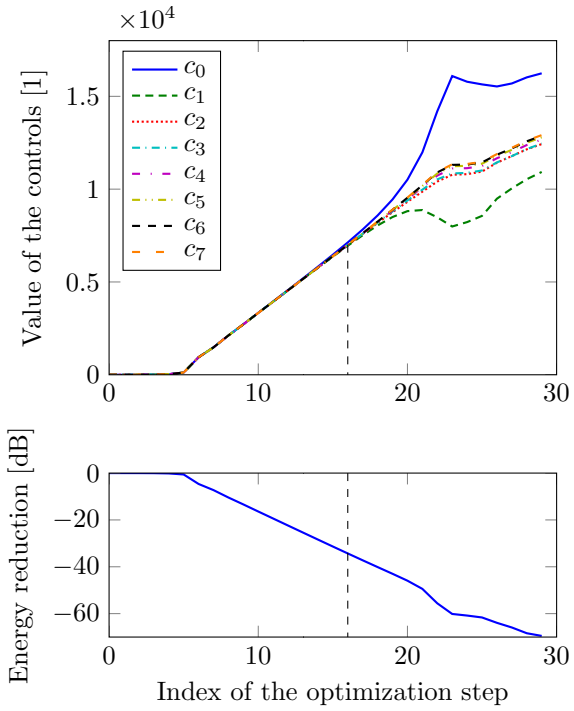

Figure 6: Evolution of controls (top) and reduction in energy (bottom) for the acoustic wave example as a function of the iteration step during the optimisation process for calibrating a piecewise-constant attenuation function with eight controls on a 0.08 m wide perfectly matched layer.

a 0.08 m wide PML together with the corresponding reduction in energy. For up to approximately 17 iterations the process favours a constant AF. From the point at which the AF deviates significantly from a constant AF, a further 20dB to 30dB reduction in energy is observed.

6.1.2 Elastodynamic wave propagation on a square

We simulate elastic wave propagation in an isotropic, homogeneous square domain $\Omega_i = [-6, 6]^2$ mm, which is extended in both the x- and y-directions with a 6 mm wide PML (see Figure 7a). We implement reflecting fixed boundaries on all sides of the computational domain. The longitudinal wave speed in the considered medium is $v_l = 5830.95$ m/s and the transverse wave speed $v_t = 3464.10$ m/s. The mass density of the considered material is 2500 kg/m^3. A Gaussian source $\boldsymbol{f} = (f_x, 0)$ is applied, where

$$f_x = \exp\left(-\left(\frac{t - 50\Delta t}{50\Delta t/4}\right)^2\right) \exp\left(-\left(\frac{x}{10^{-6}}\right)^2\right) \exp\left(-\left(\frac{y}{10^{-6}}\right)^2\right). \tag{27}$$

A typical resulting elliptical wave front for this example is illustrated in Figure 7b.

The domain is meshed with crossed-triangle cells with edge length 1.2 mm. We solve this example using a discontinuous Galerkin finite element method, which is presented in B.2. A time step size of $\Delta t = 4 \times 10^{-8}$ s is used. The calibration time is chosen to be $T_c = t_0 + (12 \text{ mm})\sqrt{2}/c_t$, which is the time needed for the peak to enter the domain and travel to the corner of the computational domain at the lowest wave speed. We consider the problem of interest to be identical to the calibration set-up with the exception of the evaluation time. Since the calibration time doesn't allow the wave to travel once in both direction through the absorbing layer, the reduction in energy would not include the full benefit of the absorbing layer. The evaluation time for this example is $T_e = t_0 + (24 \text{ mm})\sqrt{2}/c_t$, which is the calibration time plus the time needed for the peak to travel back from the corner of the computational domain to the centre of the domain.

This model uses one AF in each spatial direction. It is however undesirable to have orientation dependent PMLs because of the symmetry of the domain. We therefore choose to define the AFs in both directions by the same control variables.

The evolution of the controls and reduction in energy at each optimiser step for the piecewise-constant case are shown in Figure 8. Despite the large changes in the control values at low iteration counts, the reduction in energy remains more-or-less constant from the second iteration. The final result is again not a monotonically increasing function, shown by the AF in Figure 9 (solid blue line).

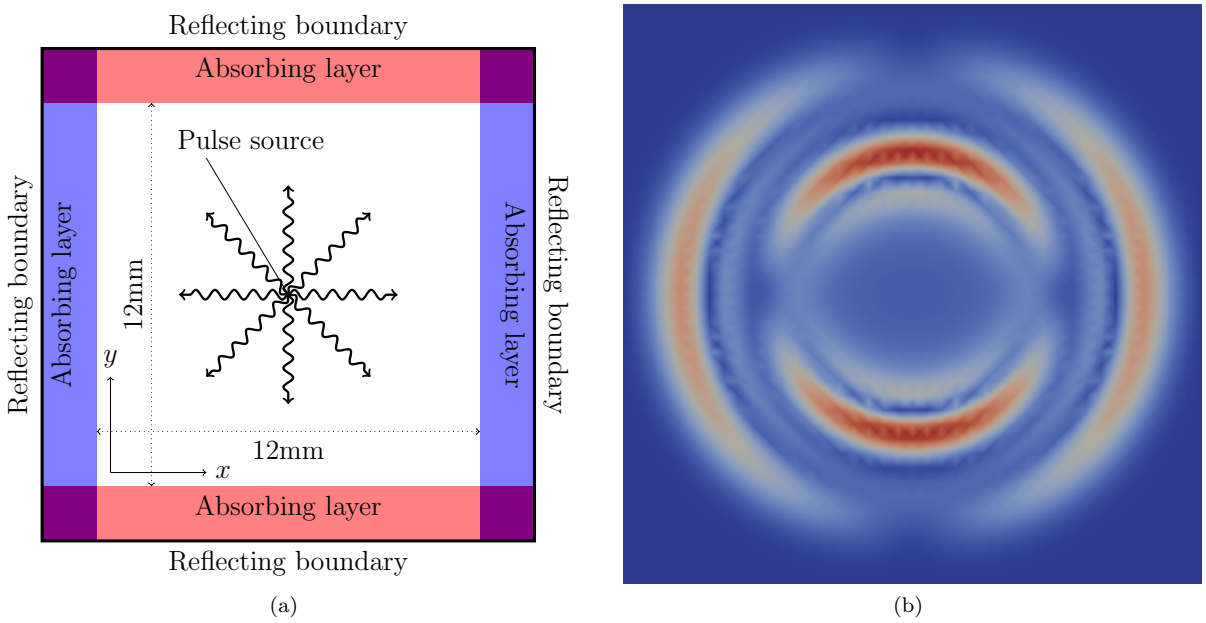

(a) (b)

Figure 7: Geometry of the elastodynamic wave example with waves propagating in radial direction (left) with typical resulting wave propagation pattern (right).

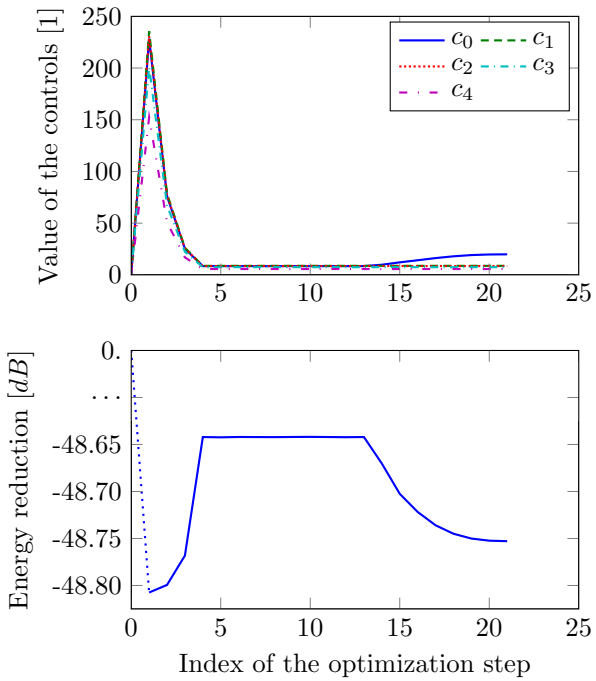

Figure 8: Evolution of the controls (top) and reduction in energy (bottom) for the elastodynamic wave example as a function of the iteration step during the calibration process for a piecewise-constant attenuation function with five parameters for a 6 mm wide perfectly matched layer.

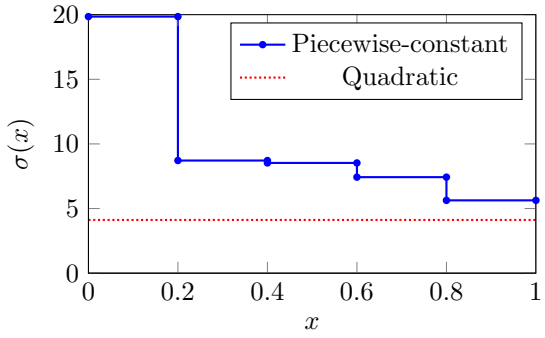

Figure 9: Piecewise-constant (solid blue) and quadratic (dotted red) attenuation function $\sigma(x)$ obtained with the calibration procedure for the elastodynamic wave example with square geometry.

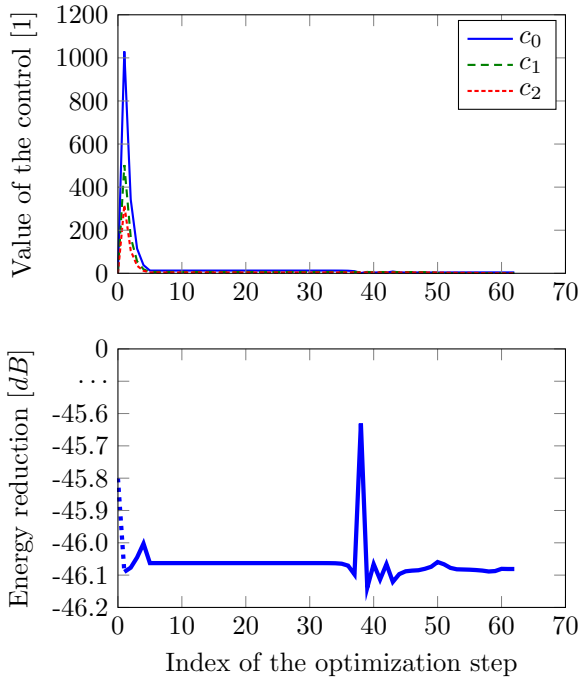

Figure 10: Evolution of the controls (top) and reduction in energy (bottom) for the elastodynamic wave example with square geometry as a function of the iteration step during the optimisation process for calibrating a quadratic attenuation function for a 6 mm wide perfectly matched layer.

As a second experiment for this model, we compare the piecewise-constant result to a quadratic AF. The evolution of the controls and reduction in energy during the optimisation process for a quadratic AF are shown in Figure 10. The calibration process for a quadratic AF has resulted in a constant AF (see Figure 9) and performs about 5% less well than the calibrated piecewise-constant AF.

6.2 Consecutive matched layers

We now move to examining the performance of the truncation strategy of consecutive matched layers presented in Section 4. In this case each 'sub-layer' has a constant attenuation function associated with it. The key difference with perfectly matched layers is the absence of auxiliary fields and equations in the model.

6.2.1 Elastodynamic wave propagation on a square

We revisit the elastodynamic example from Section 6.1.2. Both the problem of interest and the calibration set-up are identical to the previous example with the PML replaced by CMLs. The evolution of the controls and reduction in energy during the optimisation process for calibrating the five CMLs are shown in Figure 11. The results shown in Figure 11 are almost identical to the PML results in Figure 8. Since the model for CMLs does not require ADEs, in contrast to the PML model, the automatic calibration procedure for CMLs is faster than for PMLs.

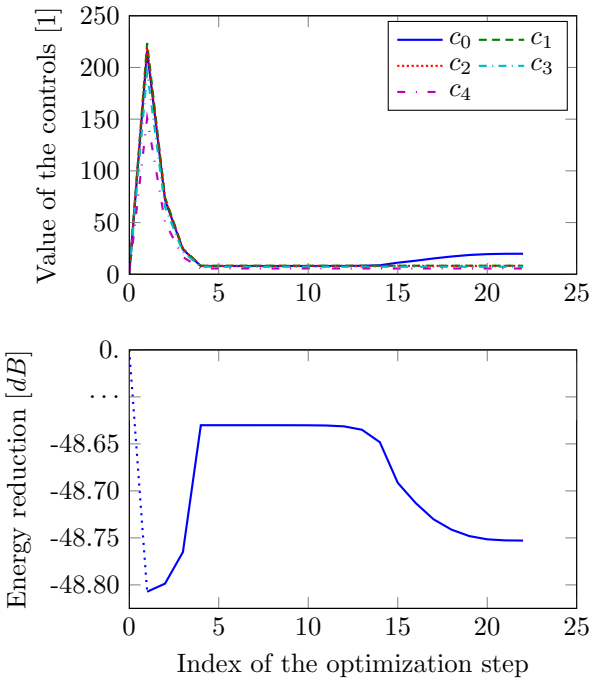

Figure 11: Evolution of the controls (top) and reduction in energy (bottom) for the elastodynamic wave example as a function of the iteration step during the bounded calibration process for consecutive matched layers.

6.2.2 Elastodynamic wave propagation on a more complicated geometry

We now adopt the problem of interest and calibration set-up of the preceding elastic example, but replace the square domain by the domain and mesh shown in Figure 12. The domain of interest is shown in dark blue. Five consecutive matched layers are placed around the domain of interest. The precise definition of the domain and the mesh are available in the supporting material [30].

The evolution of the attenuation constants for this problem and the corresponding reduction in energy are shown in Figure 13. The reduction in energy is only ten percent less than for the problem on the square domain. The attenuation in layers closer to the domain of interest is larger than for the layers farther from the domain of interest. This is probably a manifestation of the sensitivity of the different controls. It is to be expected that the attenuation in the outer layers has less effect on the reduction in energy, since a considerable amount of energy will have been damped by layers closer to the domain of interest.

6.2.3 Electromagnetic wave propagation

We consider an application for which an absorbing region is calibrated, and then used to solve a problem of interest. The problem of interest involves a transverse electromagnetic wave [18] in a parallel plate wave guide. We solve equation (3) on the domain of interest $\Omega_i = [0, L_x] \times [0, L_y] \times [0, L_z(x)]$. We consider conducting plates at $x = 0$ and $x = L_x$, which are both modelled by implementing perfect electric conducting boundary conditions ($\boldsymbol{n} \times \boldsymbol{E} = \boldsymbol{0}$) at $x = 0$ and $x = L_x$. The face at $z = 0$ is a port through which waves are inserted into the wave guide. We consider the case where the plates are infinite in y-direction, which is modelled by applying perfect magnetic conducting boundary conditions ($\boldsymbol{n} \times \boldsymbol{H} = \boldsymbol{0}$) at $y = 0$ and $y = L_y$. For $z \geq L_z(x)$ there is open space, which will be modelled using CMLs.

Before solving the problem of interest we calibrate the AFs on the adsorbing layer. To study the impact of oblique incidence angles at the boundary of the domain of interest, we will 'stretch' the upper conducting plate ($x = L_x$) in the z direction. Three configurations will be tested, i.e., with 90, 60 and 45 degree incidence angles. The domain with a 60 degree incidence angle is shown in Figure 14. The volume of absorbing layers will slightly differ in all three cases due to the different plate lengths, but the thickness of each layer (in the z-direction) is fixed.

We extend the domain of interest with five absorbing layers, each one cell wide (see Figure 14). Also the boundary conditions of the domain of interest at $x = 0$, $x = L_x$, $y = 0$ and $y = L_y$ are extended to the absorbing

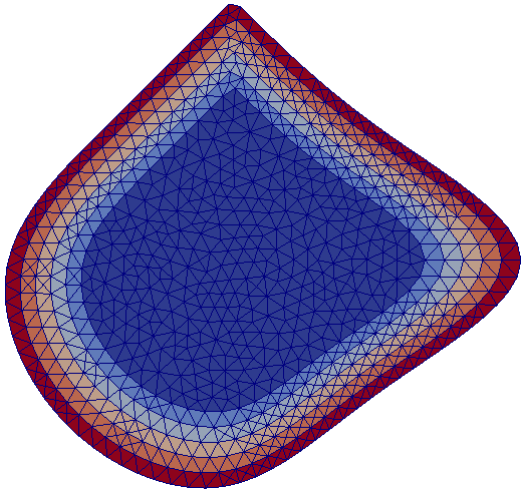

Figure 12: The more complicated computational domain used for the elastodynamic wave experiment with consecutive matched layers. The domain of interest (dark blue) is surrounded by five tightly wrapped consecutive matched layers, each indicated by a distinct colour.

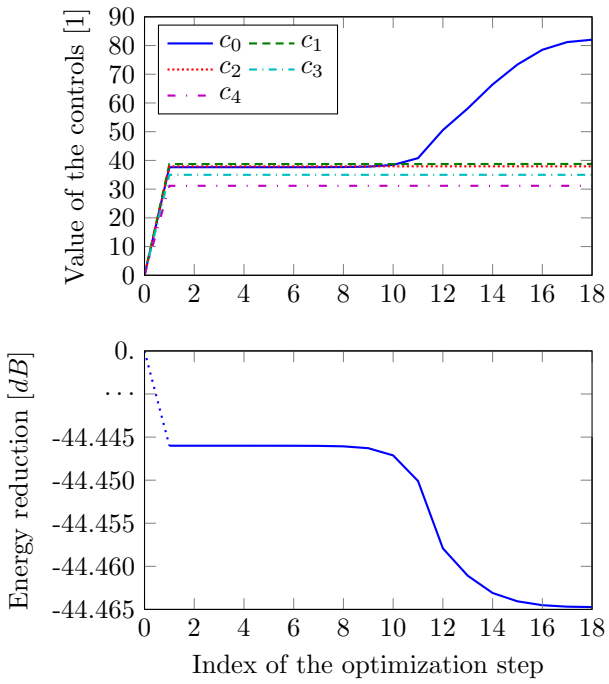

Figure 13: Evolution of the controls (top) and reduction in energy (bottom) for the elastodynamic wave example with a complicated geometry as a function of the iteration step during the calibration process for consecutive matched layers.

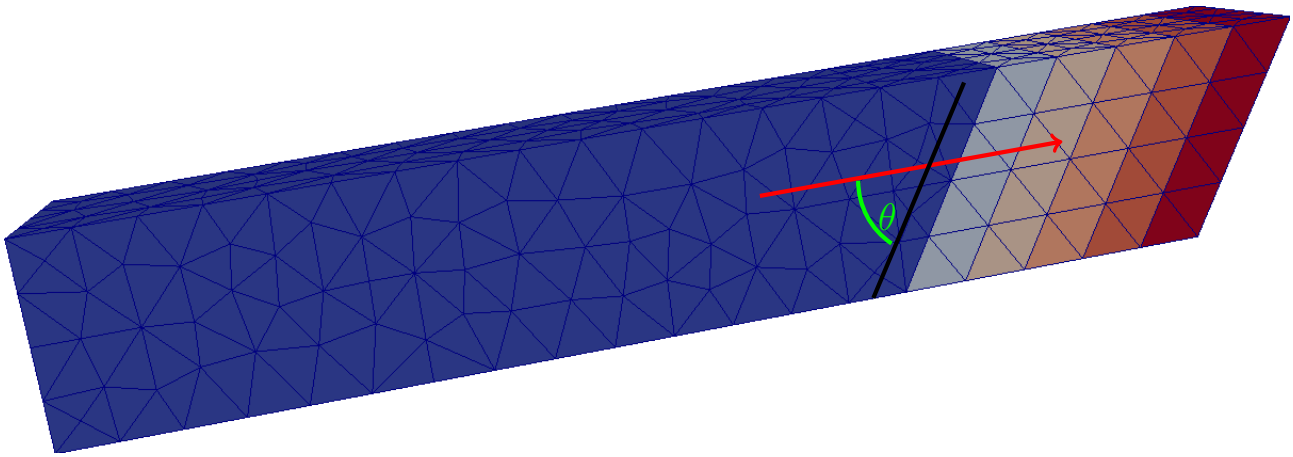

Figure 14: A parallel plate wave guide used for the electromagnetic example. The domain of interest (dark blue) is extended with five consecutive matched layers, each indicated by a different colour. In this problem, the waves enter the consecutive matched layers at a 60 degree angle θ. By modifying the length of the upper plate, the incidence angle can be controlled.

domain. The boundary condition at the port ($z = 0$) is set to $\boldsymbol{E} = (E_x, 0, 0)$, where

$$E_x(t) = \exp\left(-\left(\frac{t - 10^{-8}}{10^{-8}/4}\right)^2\right). \tag{28}$$

At the end of the CMLs ($z = L_z(x)$) a perfect electric conducting boundary condition is applied. The calibration time is chosen to be the time for the peak of the input pulse to enter the system, move through the domain of interest, reflect off the interface between the domain of interest and the absorbing domain, and back to the source of the input signal, which is $T_c = 10^{-8} + 2L_z(0)/c$. To optimise the attenuation functions, we initialise the AFs to zero, and run the optimisation process for the 90, 60 and 45 degree incidence angle cases.

The evolution of the control variables and the corresponding reduction in energy at $T_e = T_c$ for the cases with 90, 60 and 45 degree incidence angles are shown in Figure 15. We see that the two cases with non-perpendicular incidence perform well relative to the to the 90 degree case. The obtained attenuation values differ significantly between the three cases. The smaller the incidence angle, the more iterations are required to converge the optimisation algorithm.

We observe the least energy reduction for the 60 degree incidence case. The observation that the 45 degree incidence case performs better than both other cases is mainly because when a wave hits the interface between the domain of interest and the absorbing domain at a 45 degree incidence angle, the wave is reflected to the upper plate, hits it perpendicularly and hence is reflected again at a forty-five degree angle to the CMLs, before it gets reflected again in negative z-direction towards the source of the input signal. In other words, reflected waves meet the CMLs for a second time sooner than in the other cases.

To complete the electromagnetic wave case study, we compute a transverse electromagnetic wave in the wave guide with the 60 degree incidence angle and the CMLs that were calibrated for this case. The boundary conditions are as described for the calibration set-up, except now as an input wave we apply the boundary condition $\boldsymbol{E} = (E_x, 0, 0)$ at the port ($z = 0$), with

$$E_x(t) = \sin\left(3.1 \times 10^8 t\right). \tag{29}$$

There is no analytical solution available for a transverse electromagnetic wave in a parallel plate wave guide where one plate is longer than the other. However, as the waves move from left to right in the wave guide, the solution in the rectangular part $\mathcal{R} = [0, L_x] \times [0, L_y] \times [0, L_z(0)]$ is not affected by the rest of the domain. Hence, we can use the analytical solution for a parallel wave guide with equal plates for $\mathcal{R}$ which is

$$\boldsymbol{E} = \left(\sin\left(3.1 \times 10^8 z/c - 3.1 \times 10^8 t\right), 0, 0\right), \qquad \boldsymbol{H} = \left(0, \frac{1}{c\mu_0}\sin\left(3.1 \times 10^8 z/c - 3.1 \times 10^8 t\right), 0, 0\right), \tag{30}$$

where c is the speed of light and μ_0 is the permeability of vacuum.

For the initial condition, it is not straightforward to extend the analytical solution (30) into the absorbing region. Therefore, we start with a zero initial value and compare the numerical solution to the analytical solution after the problem reaches a steady state. To evaluate the numerical solution, we compare the electromagnetic

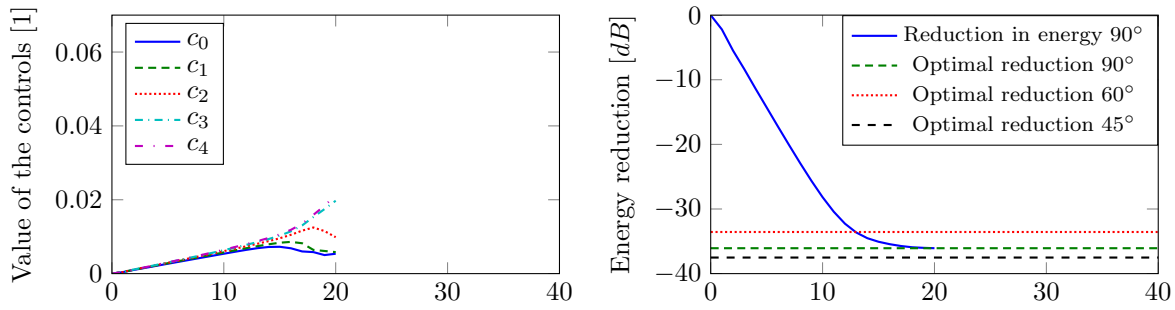

(a) 90 degree incidence.

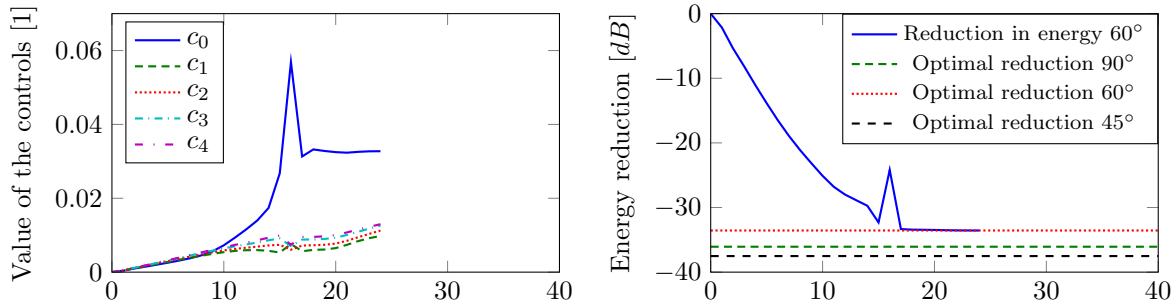

(b) 60 degree incidence.

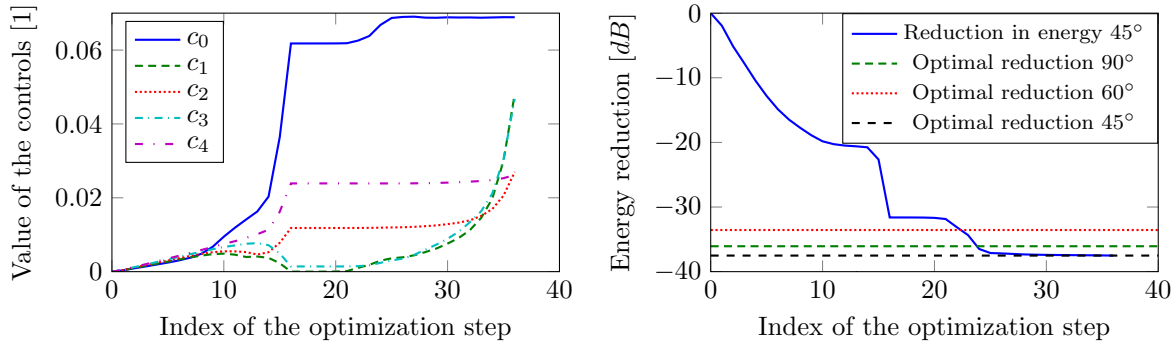

(c) 45 degree incidence

Figure 15: Evolution of the controls (left) and reduction in energy (right) for the electromagnetic wave example as a function of the iteration step during the calibration process for the consecutive matched layers for the domain with (a) 90 degree, (b) 60 degree and (c) 45 degree incidence angles.

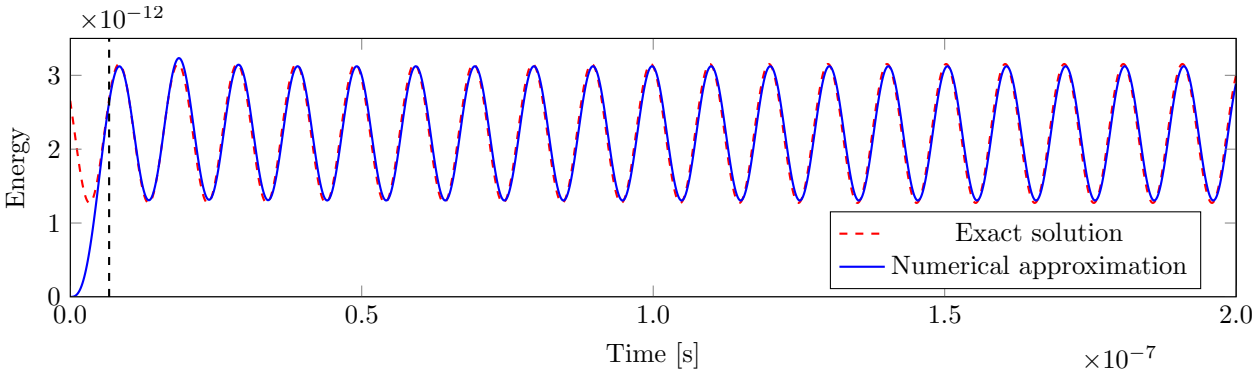

Figure 16: The computed electromagnetic energy (solid blue), as defined in (35) in a parallel plate wave guide with output port under a 60 degree angle compared to the theoretical reference (dashed red). The reference is only valid once a steady state has been reached.

energy (defined in (35)) of the numerical solution computed with third-order polynomial elements to the reference solution in (30) in $\mathcal{R}$ Figure 16. We see that, after reaching the steady state, the periods of the numerical and exact solutions are well aligned. Importantly, we see that there is no systematic increase in energy for the numerical case, which demonstrates that the CMLs are effective.

7 Conclusions

We have presented an approach to automatically calibrate attenuation functions for matched layers in wave propagation problems solved using finite element time domain methods. The presented procedure is not problem-specific, and in principle can be used to calibrate perfectly matched layers for any problem, regardless of the discretisation method. We have experimentally shown that there is no need to use polynomial attenuation functions higher than order two. Piecewise-constant attenuation functions can however result in equally effective perfectly matched layers. For piecewise-constant attenuation functions, the calibration procedure does not prefer monotonically increasing attenuation functions.

We have presented calibration of a damping strategy which we call *consecutive matched layers*. The automatic calibration procedure for consecutive matched layers is identical to the calibration procedure for perfectly matched layers. Consecutive matched layers lead to a simpler model than perfectly matched layers, resulting in shorter simulation times, for both the forward problem and the calibration procedure. It was shown for a collection of examples that consecutive matched layers can perform as well as perfectly matched layers. As a major advantage of consecutive matched layers over perfectly matched layers is that consecutive matched layers can be easily applied to complex domains.

Acknowledgements

The authors would like to acknowledge Febe Brackx for her help with the preliminary implementation and simulations, Patrick Farrell and Simon Funke for their assistance with dolfin-adjoint, Stefan Vandewalle, for helpful discussions on the content of this paper. Steven Vandekerckhove was been funded by a PhD grant from the Agency for Innovation by Science and Technology (IWT) and an international collaboration grant from the Research Foundation - Flanders (FWO).

References

References

[1] M. S. Alnæs, A. Logg, K. B. Ølgaard, M. E. Rognes, and G. N. Wells. Unified Form Language: A domain-specific language for weak formulations of partial differential equations. *ACM Trans Math Software*, 40(2): 9:1–9:37, 2014.

[2] M. S. Alnæs, J. Blechta, J. Hake, J. Johansson, B. Kehlet, A. Logg, C. Richardson, J. Ring, M. E. Rognes, and G. N. Wells. The FEniCS Project Version 1.5. *Archive of Numerical Software*, 3(100):9–23, 2015.

[3] S. Asvadurov, V. Druskin, M. Guddati, and L. Knizhnerman. On optimal finite-difference approximation of PML. *SIAM Journal on Numerical Analysis*, 41(1):287–305, 2003.

[4] J.-P. Bérenger. A perfectly matched layer for the absorption of electromagnetic waves. *Journal of Computational Physics*, 114(2):185 – 200, 1994.

[5] O. Bou Matar, P.-Y. Guerder, Y. Li, B. Vandewoestyne, and K. Van Den Abeele. A nodal discontinuous Galerkin finite element method for nonlinear elastic wave propagation. *The Journal of the Acoustical Society of America*, 131(5):3650–3663, 2012.

[6] R. H. Byrd, P. Lu, and J. Nocedal. A limited memory algorithm for bound constrained optimization. *SIAM Journal on Scientific and Statistical Computing*, 16, 5:1190–1208, 1995.

[7] W. C. Chew and J. M. Jin. Perfectly matched layers in the discretized space: An analysis and optimization. *Electromagnetics*, 16(4):325–340, 1996.

[8] W. C. Chew and W. H. Weedon. A 3-d perfectly matched medium from modified Maxwell's equations with stretched coordinates. *Micro. Opt. Tech. Lett.*, 7(13):599–604, 1994.

[9] F. Collino and P. B. Monk. Optimizing the perfectly matched layer. *Computer Methods in Applied Mechanics and Engineering*, 164(12):157 – 171, 1998.

[10] B. Engquist and A. Majda. Absorbing boundary conditions for numerical simulation of waves. *Proceedings of the National Academy of Sciences*, 74(5):1765–1766, 1977.

[11] V. Etienne, E. Chaljub, J. Virieux, and N. Glinsky. An hp-adaptive discontinuous Galerkin finite-element method for 3-D elastic wave modelling. *Geophysical Journal International*, 183(2):941–962, 2010.

[12] P. E. Farrell, D. A. Ham, S. W. Funke, and M. E. Rognes. Automated derivation of the adjoint of high-level transient finite element programs. *SIAM Journal on Scientific Computing*, 35(4):C369–C393, 2013.

[13] S. W. Funke and P. E. Farrell. A framework for automated PDE-constrained optimisation. *submitted*, 2013. arXiv:1302.3894 [cs.MS].

[14] H. Gao and J. Zhang. Implementation of perfectly matched layers in an arbitrary geometrical boundary for elastic wave modelling. *Geophysical Journal International*, 174(3):1029–1036, 2008.

[15] T. Hagstrom. Radiation boundary conditions for the numerical simulation of waves. *Acta Numerica*, 8: 47–106, 1999.

[16] J. Hesthaven and T. Warburton. *Nodal discontinuous Galerkin methods*, volume 54 of *Texts in Applied Mathematics*. Springer, Berlin, 2008.

[17] R. Holland and J. W. Williams. Total-field versus scattered-field finite-difference codes: A comparative assessment. *Nuclear Science, IEEE Transactions on*, 30(6):4583–4588, Dec 1983.

[18] J. D. Jackson. *Classical Electrodynamics*. Wiley, United States, 1998.

[19] E. Jones, T. Oliphant, P. Peterson, et al. SciPy: Open source scientific tools for Python, 2001–. URL `http://www.scipy.org/`. [Online; accessed 2014-12-02].

[20] I. Katz, D. Parks, A. Wilson, M. Rotenberg, and J. Harren. Non-reflective free space boundary conditions for SGEMP codes. *Systems, Science and Software*, SSS-R-76-2934, May 1976.

[21] A. Logg and G. N. Wells. DOLFIN: Automated finite element computing. *ACM Trans Math Software*, 37 (2):20:1–20:28, 2010.

[22] A. Logg, K.-A. Mardal, and G. N. Wells, editors. *Automated Solution of Differential Equations by the Finite Element Method*, volume 84 of *Lecture Notes in Computational Science and Engineering*. Springer, 2012.

[23] G. Mur. Absorbing boundary conditions for the finite-difference approximation of the time-domain electromagnetic-field equations. *Electromagnetic Compatibility, IEEE Transactions on*, EMC-23(4):377–382, Nov 1981.

[24] J. C. Nédélec. Mixed finite-elements in $\mathbb{R}^3$. *Numerische Mathematik*, 35(3):315–341, 1980.

[25] J. Nocedal and S. J. Wright. *Numerical optimization*. Springer, 233 Spring Street, New York, NY 10013, USA, second edition edition, 2000.

[26] A. F. Peterson. Absorbing boundary conditions for the vector wave equation. *Microwave and Optical Technology Letters*, 1(2):62–64, 1988.

[27] P. A. Raviart and J. M. Thomas. Primal hybrid finite-element methods for 2nd-order elliptic equations. *Mathematics of Computation*, 31(138):391–413, 1977.

[28] F. L. Teixeira and W. C. Chew. Complex space approach to perfectly matched layers: a review and some new developments. *International Journal of Numerical Modelling: Electronic Networks, Devices and Fields*, 13(5):441–455, 2000.

[29] F. Tröltzsch. *Optimal Control of Partial Differential Equations: Theory, Methods and Applications*. American Methematical society, Providence, Rhode Island, 2010. Graduate Studies in Mathematics, Volume 112.

[30] S Vandekerckhove. Automatic calibration of damping layers in finite element time domain simulations, January 2016. URL `http://dx.doi.org/10.5281/zenodo.45296`.

[31] K. S. Yee. Numerical solution of initial boundary value problems involving Maxwell's equations in isotropic media. *IEEE Trans. Antennas Propag.*, Vol. 14:302–307, 1966.

A Problem specific expressions

A.1 Acoustic wave propagation

The matrices $\boldsymbol{A}_i$ for the acoustic wave problem read:

$$\boldsymbol{A}_1 = \begin{pmatrix} 0 & 0 & 0 & \rho^{-1} \\ 0 & 0 & 0 & 0 \\ 0 & 0 & 0 & 0 \\ K & 0 & 0 & 0 \end{pmatrix}, \quad \boldsymbol{A}_2 = \begin{pmatrix} 0 & 0 & 0 & 0 \\ 0 & 0 & 0 & \rho^{-1} \\ 0 & 0 & 0 & 0 \\ 0 & K & 0 & 0 \end{pmatrix}, \quad \boldsymbol{A}_3 = \begin{pmatrix} 0 & 0 & 0 & 0 \\ 0 & 0 & 0 & 0 \\ 0 & 0 & 0 & \rho^{-1} \\ 0 & 0 & K & 0 \end{pmatrix}. \tag{31}$$

The energy functional for the acoustic wave problem reads:

$$E_{\text{acoustic}}(t) = \frac{1}{2} \int_\Omega \rho \boldsymbol{v} \cdot \boldsymbol{v} + \frac{1}{K} p^2 \, \mathrm{d}x \tag{32}$$

The matrix Q in (23) for this problem reads:

$$Q = \operatorname{diag}\left(\rho,\ \rho,\ \rho,\ \frac{1}{K} \right). \tag{33}$$

A.2 Electromagnetic wave propagation

The matrices $\boldsymbol{A}_i$ for the electromagnetic wave problem read:

$$\boldsymbol{A}_1 = \begin{pmatrix} 0 & 0 & 0 & 0 & 0 & 0 \\ 0 & 0 & 0 & 0 & 0 & -\mu^{-1} \\ 0 & 0 & 0 & 0 & \mu^{-1} & 0 \\ 0 & 0 & 0 & 0 & 0 & 0 \\ 0 & 0 & \varepsilon^{-1} & 0 & 0 & 0 \\ 0 & -\varepsilon^{-1} & 0 & 0 & 0 & 0 \end{pmatrix},$$

$$\boldsymbol{A}_2 = \begin{pmatrix} 0 & 0 & 0 & 0 & 0 & \mu^{-1} \\ 0 & 0 & 0 & 0 & 0 & 0 \\ 0 & 0 & 0 & -\mu^{-1} & 0 & 0 \\ 0 & 0 & -\varepsilon^{-1} & 0 & 0 & 0 \\ 0 & 0 & 0 & 0 & 0 & 0 \\ \varepsilon^{-1} & 0 & 0 & 0 & 0 & 0 \end{pmatrix},$$

$$\boldsymbol{A}_3 = \begin{pmatrix} 0 & 0 & 0 & 0 & -\mu^{-1} & 0 \\ 0 & 0 & 0 & \mu^{-1} & 0 & 0 \\ 0 & 0 & 0 & 0 & 0 & 0 \\ 0 & \varepsilon^{-1} & 0 & 0 & 0 & 0 \\ -\varepsilon^{-1} & 0 & 0 & 0 & 0 & 0 \\ 0 & 0 & 0 & 0 & 0 & 0 \end{pmatrix}. \tag{34}$$

The energy functional for the electromagnetic wave problems reads:

$$E_{\text{em}}(t) = \frac{1}{2} \int_\Omega \mu \boldsymbol{H} \cdot \boldsymbol{H} + \varepsilon \boldsymbol{E} \cdot \boldsymbol{E} \, \mathrm{d}x. \tag{35}$$

The matrix Q in (23) for this problem reads:

$$Q = \operatorname{diag}\left(\mu,\ \mu,\ \mu,\ \varepsilon,\ \varepsilon,\ \varepsilon\right). \tag{36}$$

A.3 Elastodynamic wave propagation

The matrices $\boldsymbol{A}_i$ for the elastodynamic wave problem read:

$$\boldsymbol{A}_1 = \begin{pmatrix} 0 & 0 & 0 & -\frac{c_{11}}{\rho} & -\frac{c_{12}}{\rho} & \frac{c_{13}}{\rho} & 0 & 0 & 0 \\ 0 & 0 & 0 & 0 & 0 & 0 & 0 & 0 & -\frac{c_{66}}{\rho} \\ 0 & 0 & 0 & 0 & 0 & 0 & 0 & -\frac{c_{55}}{\rho} & 0 \\ -1 & 0 & 0 & 0 & 0 & 0 & 0 & 0 & 0 \\ 0 & 0 & 0 & 0 & 0 & 0 & 0 & 0 & 0 \\ 0 & 0 & 0 & 0 & 0 & 0 & 0 & 0 & 0 \\ 0 & 0 & 0 & 0 & 0 & 0 & 0 & 0 & 0 \\ 0 & 0 & -1 & 0 & 0 & 0 & 0 & 0 & 0 \\ 0 & -1 & 0 & 0 & 0 & 0 & 0 & 0 & 0 \end{pmatrix},$$

$$\boldsymbol{A}_2 = \begin{pmatrix} 0 & 0 & 0 & 0 & 0 & 0 & 0 & 0 & -\frac{c_{66}}{\rho} \\ 0 & 0 & 0 & -\frac{c_{21}}{\rho} & -\frac{c_{22}}{\rho} & -\frac{c_{23}}{\rho} & 0 & 0 & 0 \\ 0 & 0 & 0 & 0 & 0 & 0 & -\frac{c_{44}}{\rho} & 0 & 0 \\ 0 & 0 & 0 & 0 & 0 & 0 & 0 & 0 & 0 \\ 0 & -1 & 0 & 0 & 0 & 0 & 0 & 0 & 0 \\ 0 & 0 & 0 & 0 & 0 & 0 & 0 & 0 & 0 \\ 0 & 0 & -1 & 0 & 0 & 0 & 0 & 0 & 0 \\ 0 & 0 & 0 & 0 & 0 & 0 & 0 & 0 & 0 \\ -1 & 0 & 0 & 0 & 0 & 0 & 0 & 0 & 0 \end{pmatrix},$$

$$\boldsymbol{A}_3 = \begin{pmatrix} 0 & 0 & 0 & 0 & 0 & 0 & 0 & -\frac{c_{55}}{\rho} & 0 \\ 0 & 0 & 0 & 0 & 0 & 0 & -\frac{c_{44}}{\rho} & 0 & 0 \\ 0 & 0 & 0 & -\frac{c_{31}}{\rho} & -\frac{c_{32}}{\rho} & -\frac{c_{33}}{\rho} & 0 & 0 & 0 \\ 0 & 0 & 0 & 0 & 0 & 0 & 0 & 0 & 0 \\ 0 & 0 & 0 & 0 & 0 & 0 & 0 & 0 & 0 \\ 0 & 0 & -1 & 0 & 0 & 0 & 0 & 0 & 0 \\ 0 & -1 & 0 & 0 & 0 & 0 & 0 & 0 & 0 \\ -1 & 0 & 0 & 0 & 0 & 0 & 0 & 0 & 0 \\ 0 & 0 & 0 & 0 & 0 & 0 & 0 & 0 & 0 \end{pmatrix}. \tag{37}$$

The energy functional for the elastodynamic wave problem reads:

$$E_{\text{elastic}}(t) = \frac{1}{2}\int_\Omega \rho \boldsymbol{v}\cdot\boldsymbol{v} + \boldsymbol{\mathcal{C}^{-1}}\boldsymbol{T}\cdot\boldsymbol{T}\,\mathrm{d}x. \tag{38}$$

The matrix Q in (23) for this problem reads:

$$Q = \operatorname{diag}\left(\rho,\ \rho,\ \rho,\ \boldsymbol{C}^{-1}\right), \tag{39}$$

where $\boldsymbol{C}^{-1}$ is the stiffness tensor with in Voigt notation. Note that the matrix $\boldsymbol{Q}$ is block diagonal for this case.

B Finite element formulations

This appendix contains the finite element formulations for the examples presented in Section 6. For the description of the continuous problems we refer to Section 2. Unless mentioned otherwise in the text of Section 6, linear elements are used in all cases.

B.1 Acoustic wave propagation

We consider the acoustic wave problem described in Section 6.1.1. Applying the complex coordinate stretching transformation (6), in the first dimension only, to (2) we get the continuous system

$$\begin{aligned} \frac{1}{K}\dot{p} &= -\nabla\cdot\boldsymbol{v} + \frac{\sigma_1}{K}p, \\ \rho\dot{\boldsymbol{v}} &= -\nabla p + \boldsymbol{f} + \rho\sigma_1\boldsymbol{v}. \end{aligned} \tag{40}$$

The semi-discrete finite element problem of (40) reads: find $\boldsymbol{v} \in \boldsymbol{U}$ and $p \in W$ such that

$$\begin{aligned} \int_\Omega w \frac{1}{K} \dot{p} \,\mathrm{d}x &= -\int_\Omega w \nabla \cdot \boldsymbol{v} \,\mathrm{d}x - \int_\Omega w \frac{\sigma_1}{K} p \,\mathrm{d}x \quad \forall w \in W, \\ \int_\Omega \boldsymbol{u} \cdot \rho \dot{\boldsymbol{v}} \,\mathrm{d}x &= \int_\Omega \nabla \cdot \boldsymbol{u} p \,\mathrm{d}x - \int_\Omega \boldsymbol{u} \cdot \rho \sigma_1 \boldsymbol{v} \,\mathrm{d}x + \int_\Omega \boldsymbol{u} \cdot \boldsymbol{f} \,\mathrm{d}x \quad \forall \boldsymbol{u} \in \boldsymbol{U}, \end{aligned} \tag{41}$$

where the function space $W \subset H_0^1(\Omega)$ is the usual continuous Lagrange finite element space and $\boldsymbol{U} \subset H_0(\mathrm{div}, \Omega)$ is spanned by Raviart–Thomas elements [27]. We use the same polynomial order for both finite element spaces. The classical leapfrog scheme is used to advance in time.

B.2 Elastic wave propagation

We will use the discontinuous Galerkin finite element method for the elastodynamic example. Examples of a discontinuous Galerkin finite element methods for elastic wave propagation can be found in [5, 11].

The semi-discrete discontinuous Galerkin finite element formulation for the two-dimensional generic PML description (11) on a triangulation $\mathcal{T} = \bigcup_{i=1}^{n_k} K_i$ of the computational domain Ω into n_k overlapping cells K_i, reads: find $\boldsymbol{q} \in \boldsymbol{V}$ and $\boldsymbol{r} \in \boldsymbol{V}$ such that for all triangles $K \in \mathcal{T}$

$$\begin{aligned} \sum_K \int_{K_i} \left(\dot{\boldsymbol{q}} + \sigma_{1+2}\boldsymbol{q} + \boldsymbol{r} - \boldsymbol{f}\right) \cdot \boldsymbol{l} \,\mathrm{d}x - \sum_K \int_{K_i} \left(\boldsymbol{F}_1 \cdot \boldsymbol{l}_{,1} + \boldsymbol{F}_2 \cdot \boldsymbol{l}_{,2}\right) \mathrm{d}x \\ = -\sum_K \int_{\partial K_i} \left(n_1 \boldsymbol{F}_1^* + n_2 \boldsymbol{F}_2^*\right) \cdot \boldsymbol{l} \,\mathrm{d}s \quad \forall \boldsymbol{l} \in \boldsymbol{V}, \\ \sum_K \int_{K_i} \left(\dot{\boldsymbol{r}} - \sigma_{12}\boldsymbol{q}\right) \cdot \boldsymbol{m} \,\mathrm{d}x + \sum_K \int_{K_i} \left(\sigma_2 \boldsymbol{F}_1 \cdot \boldsymbol{m}_{,1} + \sigma_1 \boldsymbol{F}_2 \cdot \boldsymbol{m}_{,2}\right) \mathrm{d}x \\ = \sum_K \int_{\partial K_i} \left(n_1 \left(\sigma_2 \boldsymbol{F}_1\right)^* + n_2 \left(\sigma_1 \boldsymbol{F}_2\right)^*\right) \cdot \boldsymbol{m} \,\mathrm{d}s \quad \forall \boldsymbol{m} \in \boldsymbol{V}, \end{aligned} \tag{42}$$

where the notation $\boldsymbol{l}_{,i} = \partial \boldsymbol{l} / \partial x_i$ implies component-wise partial differentiation of $\boldsymbol{l}$ with respect to x_i, (n_1, n_2) is the outward normal unit vector to ∂K, $\boldsymbol{F}_i^*$ is the numerical flux (defined below), $\boldsymbol{F}_i = \boldsymbol{A}_i \boldsymbol{q}$ and the used function space is

$$\boldsymbol{V} = \left\{ \boldsymbol{v} \in \left[L^2(\Omega)\right]^5 : \boldsymbol{v}|_K \in \left[P_k(K)\right]^5 \forall K \in \mathcal{T} \right\}, \tag{43}$$

where $P_k(K)$ is the space of polynomial functions of degree $k \geq 1$ on a cell K. We choose Lax–Friedrichs numerical fluxes [16, p. 34]) to complete the formulation:

$$\boldsymbol{F}_i^* = \boldsymbol{A}_i \frac{\boldsymbol{q}^+ + \boldsymbol{q}^-}{2} + \frac{C}{2}\left(n_i^+ \boldsymbol{q}^+ + n_i^- \boldsymbol{q}^-\right), \qquad \left(\sigma_j \boldsymbol{F}_i\right)^* = \boldsymbol{A}_i \frac{\sigma_j^+ \boldsymbol{q}^+ + \sigma_j^- \boldsymbol{q}^-}{2} + \frac{C}{2}\left(n_i^+ \boldsymbol{q}^+ + n_i^- \boldsymbol{q}^-\right). \tag{44}$$

where the '+' and '−' superscripts indicate the interior and exterior side of an interface and C is the greatest wave speed occurring in the problem. The trapezoidal rule is used to advance in time. All boundary conditions are enforced weakly.

B.3 Electromagnetic wave propagation

The semi-discrete finite element formulation for the electromagnetic wave propagation problem reads: find $\boldsymbol{H} \in \boldsymbol{U} \subset H(\mathrm{div}, \Omega)$ and $\boldsymbol{E} \in \boldsymbol{V} \subset H(\mathrm{curl}, \Omega)$ such that

$$\begin{aligned} \int_\Omega \boldsymbol{u} \cdot \mu \dot{\boldsymbol{H}} &= -\int_\Omega \boldsymbol{u} \cdot \nabla \times \boldsymbol{E} \,\mathrm{d}x - \int_\Omega \boldsymbol{u} \cdot \mu\sigma \boldsymbol{H} \,\mathrm{d}x \quad \forall \boldsymbol{u} \in \boldsymbol{U}, \\ \int_\Omega \boldsymbol{v} \cdot \varepsilon \dot{\boldsymbol{E}} &= \int_\Omega \nabla \times \boldsymbol{v} \cdot \boldsymbol{H} \,\mathrm{d}x - \int_\Omega \boldsymbol{v} \cdot \varepsilon\sigma \boldsymbol{E} \,\mathrm{d}x \quad \forall \boldsymbol{v} \in \boldsymbol{V}, \end{aligned} \tag{45}$$

where the function spaces $\boldsymbol{U}$ and $\boldsymbol{V}$ are spanned by Raviart–Thomas elements [27] and Nédélec elements of the first kind [24], respectively. We use the same polynomial order for both kinds of the elements. The Yee scheme [31] is used to advance in time.

C Computing the gradient of the objective functional for the time discretised problem

Consider the generic wave equation with a PML in one spatial dimension as given in (12) to be discretised in time with the implicit trapezoidal rule, with one constant matched layer added:

$$\frac{\boldsymbol{q}_{n+1}-\boldsymbol{q}_n}{\Delta t}+\boldsymbol{A}_1\left(\frac{\boldsymbol{q}'_{n+1}+\boldsymbol{q}'_n}{2}\right)+\sigma\frac{\boldsymbol{q}_{n+1}+\boldsymbol{q}_n}{2}=\boldsymbol{f}, \tag{46}$$

where $\boldsymbol{q}_n$ is the computed approximation for $\boldsymbol{q}(n\Delta t)$ and the accent indicates a spatial derivative, i.e., $\boldsymbol{q}'_n = \partial\boldsymbol{q}_n/\partial x_1$. We introduce the vector $\bar{\boldsymbol{q}} = \left(\boldsymbol{q}_0, \boldsymbol{q}_1, \ldots, \boldsymbol{q}_{n-1}, \boldsymbol{q}_n\right)$ containing the solution at each time step. To be able to study the procedure in detail, we will restrict the time integration to two steps. In that case the objective function is

$$J(\bar{\boldsymbol{q}}, \boldsymbol{u}) = \frac{1}{2}\left\langle \boldsymbol{Q}\boldsymbol{q}(t), \boldsymbol{q}(t)\right\rangle_\Omega, \tag{47}$$

and its derivative with respect to the state vector $\bar{\boldsymbol{q}}$ is

$$\frac{\partial J}{\partial \bar{\boldsymbol{q}}} = \begin{pmatrix} 0 \\ 0 \\ \boldsymbol{Q}\boldsymbol{q}_2 \end{pmatrix}. \tag{48}$$

The system of constraints in this case consists of three equations:

$$\begin{aligned}
\boldsymbol{c}_0 &= \boldsymbol{q}_0 - \boldsymbol{f}_0 = \boldsymbol{0}, \\
\boldsymbol{c}_1 &= \frac{\boldsymbol{q}_1-\boldsymbol{q}_0}{\Delta t}+\boldsymbol{A}_1\left(\frac{\boldsymbol{q}'_1+\boldsymbol{q}'_0}{2}\right)+\sigma\frac{\boldsymbol{q}_1+\boldsymbol{q}_0}{2}=0, \\
\boldsymbol{c}_2 &= \frac{\boldsymbol{q}_2-\boldsymbol{q}_1}{\Delta t}+\boldsymbol{A}_1\left(\frac{\boldsymbol{q}'_2+\boldsymbol{q}'_1}{2}\right)+\sigma\frac{\boldsymbol{q}_2+\boldsymbol{q}_1}{2}=0,
\end{aligned} \tag{49}$$

for which we can compute the Jacobian matrix

$$\frac{\partial \boldsymbol{c}}{\partial \bar{\boldsymbol{q}}} = \begin{pmatrix} \frac{\partial \boldsymbol{c}_0}{\partial \boldsymbol{q}_0} & \frac{\partial \boldsymbol{c}_1}{\partial \boldsymbol{q}_0} & \frac{\partial \boldsymbol{c}_2}{\partial \boldsymbol{q}_0} \\ \frac{\partial \boldsymbol{c}_0}{\partial \boldsymbol{q}_1} & \frac{\partial \boldsymbol{c}_1}{\partial \boldsymbol{q}_1} & \frac{\partial \boldsymbol{c}_2}{\partial \boldsymbol{q}_1} \\ \frac{\partial \boldsymbol{c}_0}{\partial \boldsymbol{q}_2} & \frac{\partial \boldsymbol{c}_1}{\partial \boldsymbol{q}_2} & \frac{\partial \boldsymbol{c}_2}{\partial \boldsymbol{q}_2} \end{pmatrix} = \begin{pmatrix} \boldsymbol{I} & \frac{\partial \boldsymbol{c}_1}{\partial \boldsymbol{q}_0} & 0 \\ 0 & \frac{\partial \boldsymbol{c}_1}{\partial \boldsymbol{q}_1} & \frac{\partial \boldsymbol{c}_2}{\partial \boldsymbol{q}_1} \\ 0 & 0 & \frac{\partial \boldsymbol{c}_2}{\partial \boldsymbol{q}_2} \end{pmatrix}, \tag{50}$$

where $\boldsymbol{I}$ is the identity matrix of size $n \times n$ where n is the length of $\boldsymbol{q}_i$. To determine this matrix, four non-trivial partial derivatives have to be computed. In general, all we need is

$$\begin{aligned}
\frac{\partial \boldsymbol{c}_i}{\partial \boldsymbol{q}_i} &= \frac{\boldsymbol{I}}{\Delta t}+\boldsymbol{A}_1\left(\frac{\boldsymbol{D}}{2}\right)+\sigma\frac{\boldsymbol{I}}{2}, \\
\frac{\partial \boldsymbol{c}_i}{\partial \boldsymbol{q}_{i-1}} &= -\frac{\boldsymbol{I}}{\Delta t}+\boldsymbol{A}_1\left(\frac{\boldsymbol{D}}{2}\right)+\sigma\frac{\boldsymbol{I}}{2},
\end{aligned} \tag{51}$$

where $\boldsymbol{D}$ is a diagonal matrix with $\boldsymbol{D}_{ii} = \partial_{x_1}$ This information allows us to compute the adjoint states $\boldsymbol{\lambda}$ by solving

$$\frac{\partial \boldsymbol{c}}{\partial \bar{\boldsymbol{q}}}\boldsymbol{\lambda} = -\frac{\partial J}{\partial \bar{\boldsymbol{q}}}, \tag{52}$$

which in this case looks like

$$\begin{pmatrix} \boldsymbol{I} & \frac{\partial \boldsymbol{c}_1}{\partial \boldsymbol{q}_0} & 0 \\ 0 & \frac{\partial \boldsymbol{c}_1}{\partial \boldsymbol{q}_1} & \frac{\partial \boldsymbol{c}_2}{\partial \boldsymbol{q}_1} \\ 0 & 0 & \frac{\partial \boldsymbol{c}_2}{\partial \boldsymbol{q}_2} \end{pmatrix} \begin{pmatrix} \boldsymbol{\lambda}_0 \\ \boldsymbol{\lambda}_1 \\ \boldsymbol{\lambda}_2 \end{pmatrix} = - \begin{pmatrix} 0 \\ 0 \\ \boldsymbol{q}_2 \end{pmatrix}. \tag{53}$$

Solving this system by back substitution leads to

$$\begin{aligned}
0 &= \boldsymbol{\lambda}_2 + \boldsymbol{q}_2, \\
0 &= \frac{\boldsymbol{\lambda}_1-\boldsymbol{\lambda}_2}{\Delta t}+\boldsymbol{A}_1\left(\frac{\boldsymbol{\lambda}'_1+\boldsymbol{\lambda}'_2}{2}\right)+\sigma\frac{\boldsymbol{\lambda}_1+\boldsymbol{\lambda}_2}{2}, \\
0 &= \frac{\boldsymbol{\lambda}_0-\boldsymbol{\lambda}_1}{\Delta t}+\boldsymbol{A}_1\left(\frac{\boldsymbol{\lambda}'_0+\boldsymbol{\lambda}'_1}{2}\right)+\sigma\frac{\boldsymbol{\lambda}_0+\boldsymbol{\lambda}_1}{2},
\end{aligned} \tag{54}$$

which is identical to solving the forward problem (49) up to the variable names. In fact, by feeding $-\boldsymbol{q}_2$ to the forward solver as a source, the adjoint states will be computed in reversed order.

To obtain the gradient, all that remains is to multiply the forward and adjoint states:

$$\frac{\mathrm{d}J}{\mathrm{d}\boldsymbol{u}} = \sum_{i=0}^{n} \left\langle \boldsymbol{\lambda}_i^T, \boldsymbol{q}_i \right\rangle . \tag{55}$$